Evaluation of CO2 Hydrate Saturation in Porous Core Experiments Using Medical CT Images

Aghajanloo, M.; Jones, S.; Yan, L.; Voskov, D.; Farajzadeh, R.

DOI
10.1021/acs.energyfuels.4c01537

Publication date
2023

Document Version
Final published version

Published in
Energy & Fuels

Citation (APA)
Aghajanloo, M., Jones, S., Yan, L., Voskov, D., & Farajzadeh, R. (2023). Evaluation of CO2 Hydrate Saturation in Porous Core Experiments Using Medical CT Images. *Energy & Fuels*, *38*(12), 11037−11042. https://doi.org/10.1021/acs.energyfuels.4c01537

energy&fuels

Open Access

pubs.acs.org/EF

Article

Evaluation of CO_2 Hydrate Saturation in Porous Core Experiments Using Medical CT Images

M. Aghajanloo,* S. Jones, L. Yan, D. Voskov, and R. Farajzadeh

Cite This: *Energy Fuels* 2024, 38, 11037−11042

Read Online

ACCESS | Metrics & More | Article Recommendations

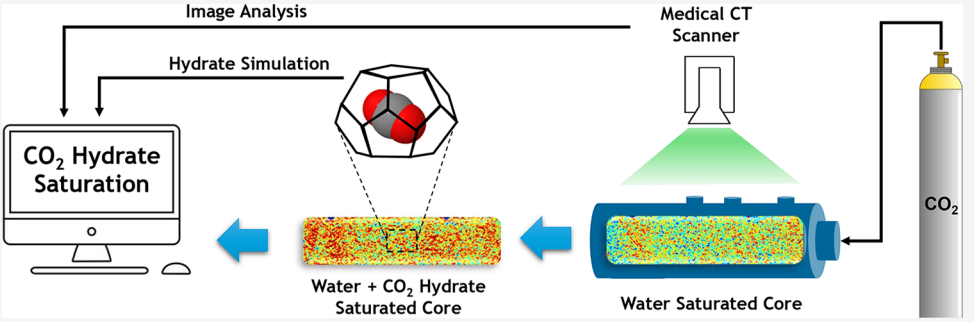

ABSTRACT: Understanding the kinetics of CO_2 hydrate formation and the resulting saturation of the hydrate in porous rocks is crucial for processes such as the storage of CO_2 in underground formations. Nevertheless, to date, there is no established procedure that utilizes a medical CT scanner for quantifying gas hydrate saturation in core samples during the growth stage. This study proposes a methodology for estimating hydrate saturation using a medical CT scanner during the injection of CO_2 into porous media. This method uses the mean area obtained from the image analysis to calculate the dynamic profile of water and the CO_2 hydrate along the length of the sandstone core. To demonstrate the technique, core flooding experiments were conducted to form gas hydrates in semibrine-saturated sandstone cores.

1. INTRODUCTION

In the carbon capture and storage chain, depleted hydrocarbon reservoirs are attractive options for CO_2 storage, given their available infrastructure, proven capacity, and safe long-term storage.[1,2] However, dynamic coupled mass and heat transfer models have shown that there can be a phase transition from liquid or gas CO_2 into CO_2 hydrate during the high-pressure injection of CO_2 into depleted gas reservoirs.[3] In this scenario, predicting the kinetics behavior of CO_2 hydrate poses challenges due to its generation and dissociation being contingent on reservoir thermodynamic conditions and the stability of CO_2 hydrate. The stability of the CO_2 hydrate is influenced by several factors such as the CO_2 solubility and hydrate density.[4−6] In contrast to CO_2-limited conditions, where CO_2 is insufficient to saturate water and leads to a low water-to-hydrate conversion, the presence of excess CO_2 allows it to fully saturate the aqueous phase, which results in the formation of denser and more stable CO_2 hydrate.[7]

In the context of porous media, the dynamic behavior of CO_2 hydrate formation, saturation, and distribution needs to be determined for CO_2 hydrate formation/saturation depending on the intrinsic permeability of the porous media, the water distribution, availability of nucleation sites, and the growth kinetics of hydrate formation.[8−11] To address these challenges, visualization methods serve as a promising approach to quantitatively characterize the water−hydrate saturation of porous media under various permeabilities and predict approximate trends. So far, extensive research has utilized nondestructive methods such as MRI[12,13] and micro-CT scanning[14] to distinguish the phase states of water, gas, and gas hydrate, and estimate hydrate saturation. However, there has been no quantitative evaluation of these factors based on medical CT scanning.

Given the restricted accessibility to MRI and micro-CT equipment in many research areas and laboratories, this study proposes a methodology to quantify CO_2 hydrate saturation and density using a medical CT scanner. Both micro-CT and medical CT scanners operate using the same techniques to carry out X-ray imaging in 3D. However, there is an order of magnitude difference in resolution between medical CT and micro-CT images, and the higher resolution of micro-CT images

Received: April 1, 2024
Revised: May 18, 2024
Accepted: May 23, 2024
Published: May 31, 2024

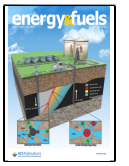

https://doi.org/10.1021/acs.energyfuels.4c01537
Energy Fuels 2024, 38, 11037−11042

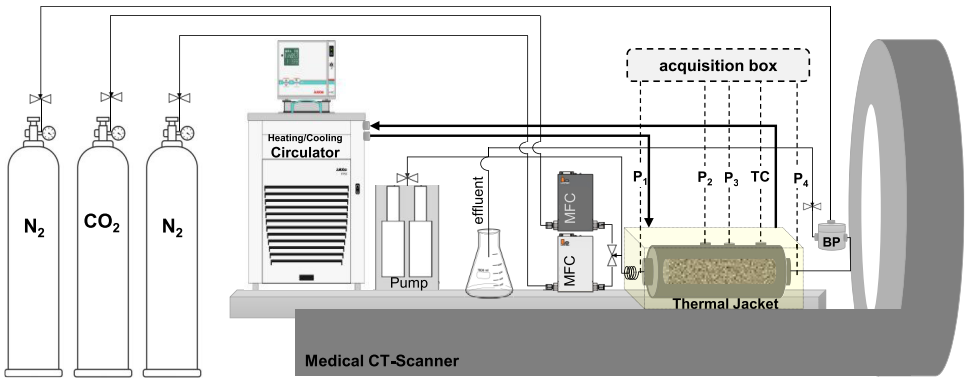

Figure 1. Schematic of the core flood gas hydrate production system with a medical CT scanner. BP, back pressure; MFC, mass flow controller; P, pressure transducer; TC, thermocouple.

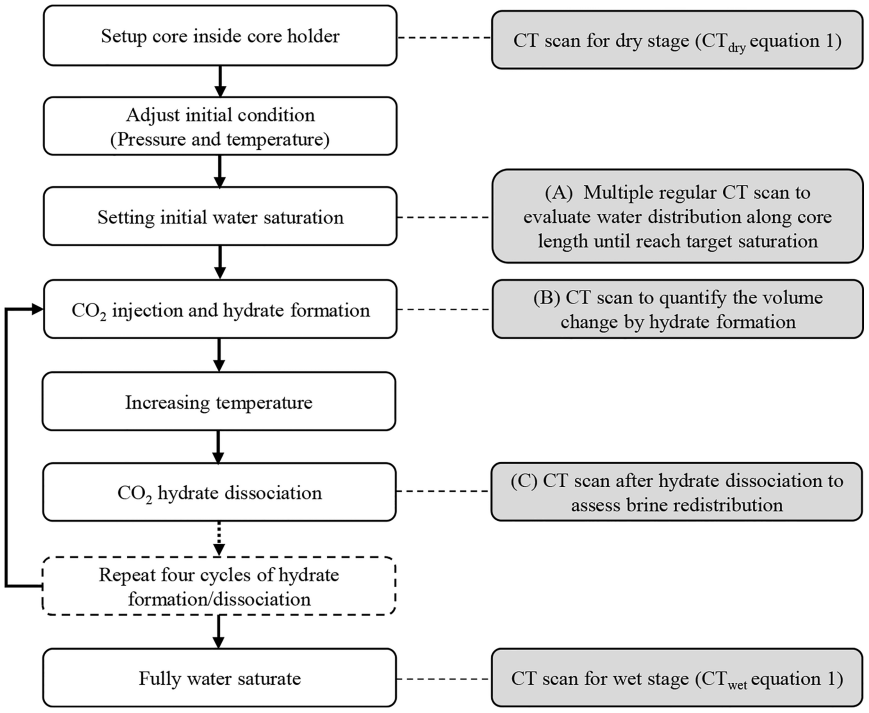

Figure 2. Flowchart of the sequential steps of the gas hydrate experiment, including CT scanning points to obtain (A) water distribution homogeneity after initial saturation, (B) gas hydrate distribution and volume, and (C) brine redistribution after dissociation.

enables the visualization of pores and grains within a rock, allowing for exact measurements of fluid saturations. In contrast, medical CT images show average information over a region of the rock structure. Typically, medical CT scanners are unable to distinguish the individual gas hydrate phase due to its close density to the water phase, but the current technique involves some additional processing, which allows the gas hydrate saturation to be calculated. This processing then allows for monitoring the CO_2 hydrate generation and decomposition process under various water saturations in a sandstone core. The practical implications of these findings are expected to be particularly pertinent and useful for scenarios such as subsurface CO_2 sequestration.

2. METHODOLOGY

2.1. Core Flood Experiments under Medical CT Scanning. The apparatus (see Figure 1), material, and experimental procedure were described in detail in our previous study.[15] In brief, the system was pressurized to 3 MPa under N_2 flow using a back pressure regulator at the core outlet (BP in Figure 1). Subsequently, N_2 and degassed brine solution containing 1 wt % NaCl were simultaneously coinjected into the core using a specific gas/water fractional flow (f_g/f_w)[16] to establish the desired brine saturation ($S_w \sim 35\%$). After N_2-brine coinjection was stopped, CO_2 injection into the core was then commenced at a constant rate of 1 mL/min at a temperature of 273.7 ± 0.5 K (here, we assume ~6.5° of subcooling based on the pure CO_2 phase diagram in the presence of 1 wt % NaCl solution, representing the temperature difference from the equilibrium condition based on bulk). Since the solubility of N_2 in water is quite small compared to that of CO_2, especially under low temperatures, it is expected that nearly all of the N_2 is purged and replaced by CO_2 soon after injection starts. However, if a small amount of N_2 remained, it would not have a considerable impact on CO_2 hydrate PT diagram at the aforementioned experimental condition (30 bar and 273.7 K).[11]

The pressure was kept constant (3 MPa) during the CO_2 injection process by using a back pressure at the core outlet.

https://doi.org/10.1021/acs.energyfuels.4c01537
Energy Fuels 2024, 38, 11037−11042

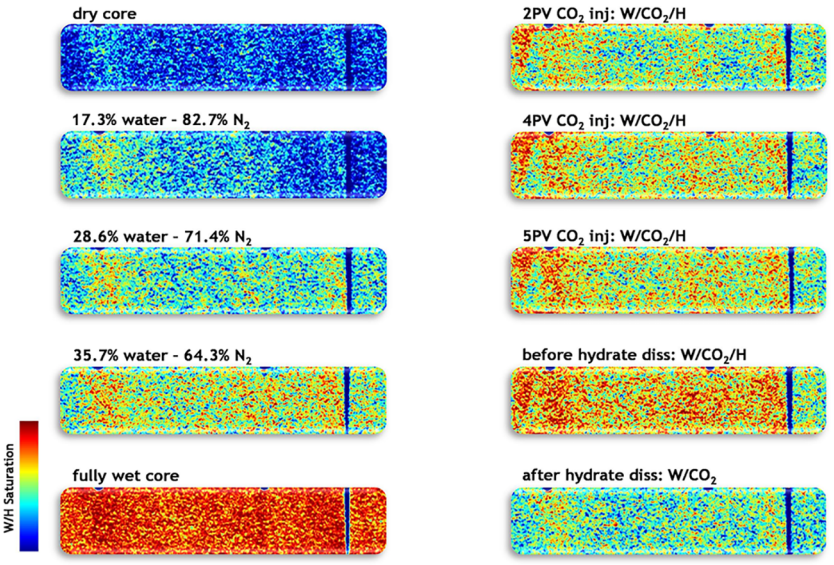

Figure 3. Qualitative CT images of the water+hydrate saturation within a Bentheimer core. The left-hand column shows images obtained during the initial water saturation step, as well as the end-point dry and wet scans. The right column shows images obtained during the hydrate formation and dissociation steps. In each case, the fluid flow direction is from left to right along the core.

Furthermore, due to the low water saturation and the effect of capillary pressure, brine production was not observed from the core during the process of N_2 injection or when switching from N_2 to CO_2. The CO_2 injection continued until maximum hydrate formation and a steady state were achieved, after which dissociation was initiated through thermal stimulation. Cyclic hydrate formation/dissociation was carried out to assess the water memory effect and the impact of hydrate formation and dissociation on water/hydrate redistribution. The dissociation temperature remained below 293.15 K, and the dissociation process was completed within 1 day, ensuring that the maximum memory effect was preserved.

The procedure for the whole experiment, indicating the repeat cycles, is summarized in the flowchart in Figure 2.

The medical CT scanner (dual-source Siemens Somatom Definition) was utilized to quantify the saturations of the three phases (water/hydrate/gas) at specific points in the experimental process, as indicated in Figure 2. The scanner gives a slice thickness of 0.6 mm and a resolution of 0.3 mm when using a 150-mm field of view, resulting in images with a voxel size of 0.3 × 0.3 × 0.6 mm.

2.2. Data Acquisition and Processing. The processing of the gas hydrate saturation data obtained from the medical CT scan involves analyzing the CT images to identify and measure the volume or saturation of gas hydrates within the scanned sandstone core.[17] The following steps outline the methodology for calculating gas hydrate saturation using medical CT scans:

(1) The CT images are imported as a stack into an image processing package. In the current case, ImageJ was used, but the analysis can be carried out using any software package capable of performing image subtraction.

(2) Cropping the image to extract the region of interest, enclosing the area containing the core along with gas hydrates and water, and applying this for all groups of images to enhance the accuracy of the calculation.

(3) Differentiation of water−gas hydrate (due to the similar density of water and CO_2 hydrate) within each region of the core based on their distinct density and CT numbers compared to rock and gas. The water + gas hydrate saturations can then be calculated by comparing the CT values at each step of the experiment (CT_{exp}) to both fully water-saturated (CT_{wet}) and completely dry (CT_{dry}) conditions, using the following equation:[8]

$$S_{w+H} = \frac{CT_{exp} - CT_{dry}}{CT_{wet} - CT_{dry}} \quad (1)$$

To minimize the noise in the measurements, the saturation values were then averaged by grouping the slices into sections of 1 cm in length. An average saturation for each cm along the core was then obtained.

(4) Since eq 1 yields the total saturation of water and hydrate together, the most important step in this methodology involves estimating the fraction of water converted to hydrate (f_{conv}) during the experiment based on the thermodynamic conditions. This step enables the calculation of the CO_2 hydrate saturation, S_H. The estimation of f_{conv} is determined through the presimulation of CO_2 hydrate formation using HydraFLASH, according to the thermodynamic conditions of the experiment. By incorporating this information into eq 2, the gas hydrate saturation in each section of the core length can be calculated as follows:

$$S_H = S_{w+H} - (1 - f_{conv}) \times S_w^{initial} \quad (2)$$

where $S_{w+H}(\%)$, was calculated from the image processing, using eq 1. The term $S_w^{initial}$ denotes the initial water saturation before gas hydrate formation within the core. Hydrate saturation, S_H, was defined as the hydrate volume normalized to the pore volume of the porous rock (V_φ).

In addition, once the hydrate saturation is known, the mass density of hydrate (ρ_H) can then be determined by considering the mass of water and gas contributing to the hydrate structure relative to the hydrate volume. This calculation was carried out utilizing the following equation:[18]

$$\rho_H = \frac{f_{conv} \times n_{H_2O}\left[M_w^{H_2O} + \frac{M_w^{CO_2}}{N_H}\right]}{S_H \times V_\varphi} \quad (3)$$

https://doi.org/10.1021/acs.energyfuels.4c01537
Energy Fuels 2024, 38, 11037−11042

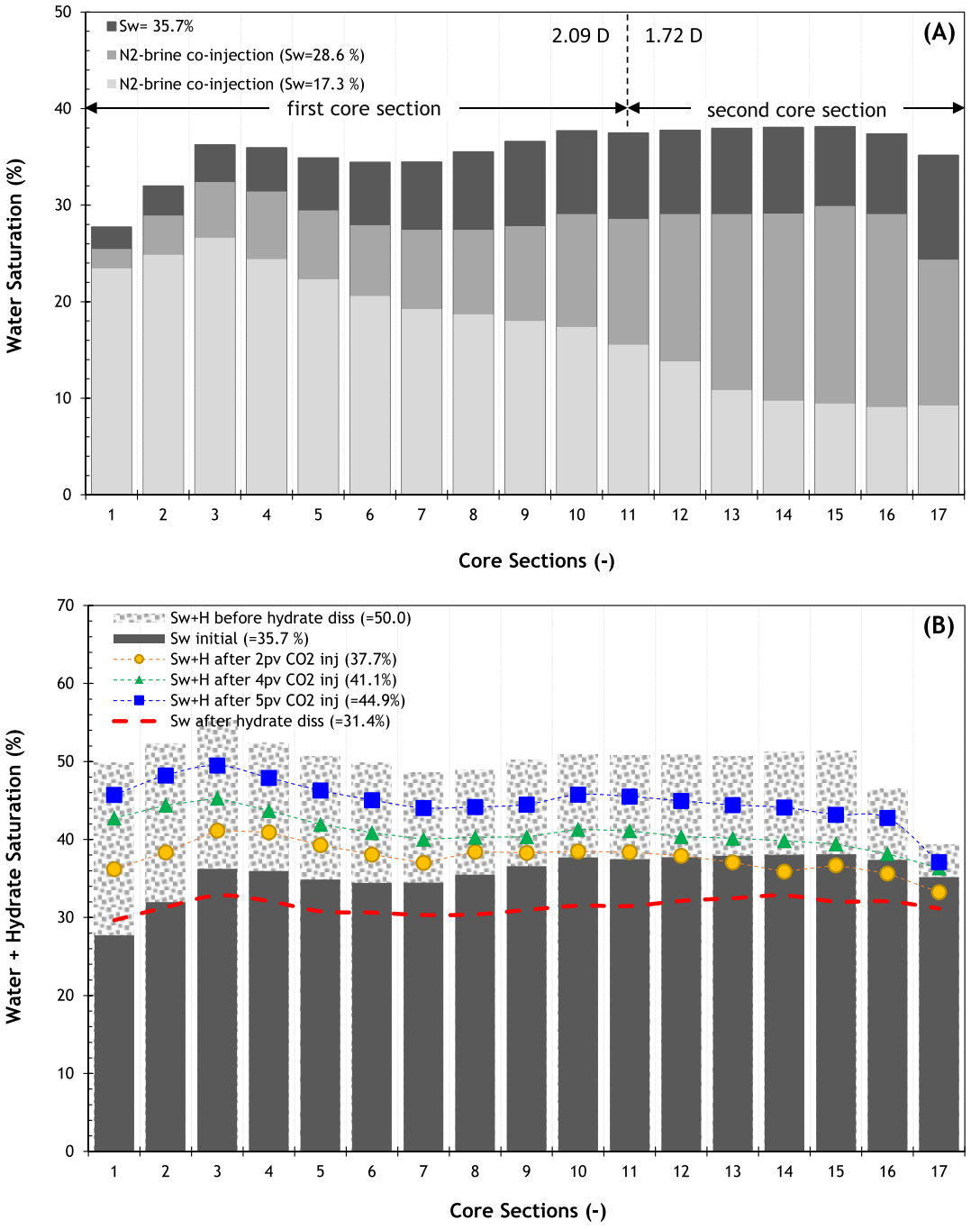

Figure 4. Saturation profiles along the Bentheimer core (17 cm length, 3.8 diameter, and 23% porosity) during (A) water saturation process, (B) CO_2 injection (hydrate formation), and hydrate dissociation. PV indicated 44.3 mL based on the core porosity volume.

Here, n_{H_2O} stands for the total moles of water initially present within the core (introduced during water saturation), and $M_w^{H_2O}$ and $M_w^{CO_2}$ represent the molecular weights of water and CO_2, respectively. The term N_H represents the hydration number and signifies the average number of water molecules per guest gas molecule that contribute to a unit hydrate structure sI.

3. RESULTS AND DISCUSSION

3.1. Determination of Water/Hydrate Saturations Using Medical CT Scan. The CT images scanned during the entire process of sample core flooding experiment, including water saturation progress, hydrate formation, and postthermal stimulation dissociation, are depicted in Figure 3. The colors qualitatively represent water/hydrate saturation, with low to high saturation indicated by blue to red color, respectively.

An assessment of the permeability of the core was conducted both before and after the experiment to evaluate the impact of hydrate formation and dissociation on core permeability. Initially, the intrinsic permeability of the core was 2.09 D over the first 10.5 cm (first core section, from inlet to P_3) and 1.72 D over the subsequent 6.5 cm (second core section, from P_3 to outlet). This difference in permeability is attributed to the inherent heterogeneously laminated structure of the sandstone core. As indicated in Figure 4A, it can be deduced that during the onset of water saturation (S_w = 17.3%), the water predominantly occupies the first section of the core where the permeability is

https://doi.org/10.1021/acs.energyfuels.4c01537
Energy Fuels 2024, 38, 11037−11042

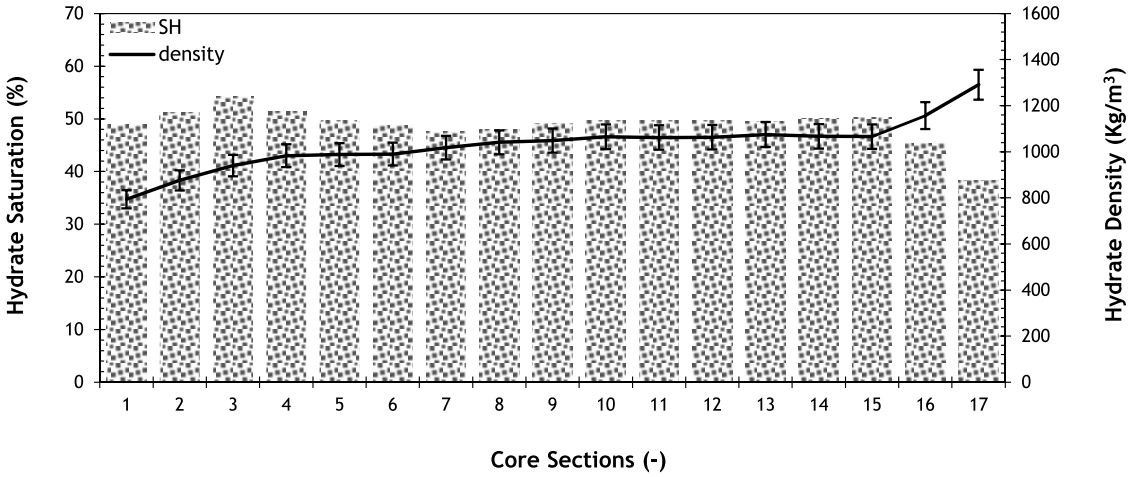

Figure 5. Final hydrate saturation and hydrate density along the Bentheimer core, considering an estimated 97% water-to-hydrate conversion and hydration number of 6.08 for hydrate structure I. The estimation is obtained using the HydraFLASH software and applying the CPA EoS under the conditions of 3 MPa, 273.7 K, and excess CO_2. The error bar represents 5%.

higher. As the water saturation level rises, there is an observable enhancement in the uniformity of water distribution along the entire length of the core, except for the first 2 cm, where saturation is lower due to the N_2 stream.

During the hydrate formation phase of the experiment, the analysis reveals a lower saturation of hydrate in the section of the core with lower permeability, as depicted in Figure 4B. This occurrence is partly attributed to the relatively higher initial water saturation in the lower permeability section of the core. The lower permeability also means that this region of the core is characterized by smaller pore spaces than the higher permeability region, and these small pore spaces then reduce the gas−water interface area, which, in turn, affects the hydrate growth.

In addition, during CO_2 injection, as observed in the 2PV, 4PV, and 5PV curves in Figure 4B, the hydrate saturation gradually increases with the rising CO_2 content in the core. This is because the CO_2 saturation in the core was initially low during the hydrate formation step, as this was preceded by several N_2 injection steps (the saturation and cooling processes). As the CO_2 concentration in the gas phase increases, the hydrate formation process maintains a relatively high driving force,[19] reaching a steady state with maximum hydrate stability, indicating the highest gas encapsulation inside the hydrate structures.

Finally, the permeability data following hydrate dissociation indicate only a slight alteration in the rock permeability when compared to the initial values.

In the specific conditions outlined in this study, characterized by the presence of excess CO_2 due to dynamic CO_2 injection and uniform water distribution, a substantial gas−water interface area is ensured. Furthermore, considering prolonged CO_2 injection, hydrate formation eventually reaches a stable state, leading to the expected maximum hydrate volume/saturation. Under the aforementioned conditions, with approximately equal input and output of CO_2 injected (near-equilibrium condition), mass transfer due to hydrate formation is negligible. In this regard, at the final stage of hydrate formation, wherein the hydrate encapsulates the maximum gas molecules and attains high stability, the estimated hydration number is 6.08. Furthermore, over 97% of the water phase is anticipated to undergo conversion to the CO_2 hydrate phase. This estimation is derived using the HydraFLASH software, applying the Cubic Plus Association (CPA) equation of state (EoS) under 3 MPa and 273.7 K. Subsequently, hydrate saturation and hydrate density were estimated employing eqs 2 and 3, respectively, as illustrated in Figure 5. The obtained results align well with the literature.[20]

4. CONCLUSIONS

To the knowledge of the authors, a well-established medical CT scan methodology specifically tailored for calculating gas hydrate saturation is absent in lab experiments. The current work has innovatively developed a new methodology that utilizes medical CT scans to accurately determine the CO_2 hydrate volume and density. This technique has been demonstrated to work for calculations of CO_2 hydrate saturation in partially water-saturated cores, as presented here, but it has the potential to be expanded for use with any gas hydrate saturation. This approach enables the utilization of core flood tests to estimate the dynamic profile of water/CO_2 hydrate saturation along the length of the core sample.

AUTHOR INFORMATION

Corresponding Author

M. Aghajanloo − *Department of Geoscience and Engineering, Delft University of Technology, 2628 CN Delft, The Netherlands;* orcid.org/0000-0001-7215-4250; Email: M.Aghajanloo@tudelft.nl

Authors

S. Jones − *Department of Geoscience and Engineering, Delft University of Technology, 2628 CN Delft, The Netherlands;* orcid.org/0000-0002-2374-8391

L. Yan − *Department of Geoscience and Engineering, Delft University of Technology, 2628 CN Delft, The Netherlands;* orcid.org/0000-0001-8774-3357

D. Voskov − *Department of Geoscience and Engineering, Delft University of Technology, 2628 CN Delft, The Netherlands; Department of Energy Science and Engineering, Stanford University, Stanford, California 94305, United States*

R. Farajzadeh − *Department of Geoscience and Engineering, Delft University of Technology, 2628 CN Delft, The Netherlands; Shell Global Solutions International B.V., 1031*

https://doi.org/10.1021/acs.energyfuels.4c01537
Energy Fuels 2024, 38, 11037−11042

HW Amsterdam, The Netherlands; orcid.org/0000-0003-3497-0526

Complete contact information is available at: https://pubs.acs.org/10.1021/acs.energyfuels.4c01537

Notes

The authors declare no competing financial interest.

■ ACKNOWLEDGMENTS

The authors thank Shell Global Solutions International for granting permission to publish this work.

■ NOMENCLATURE

BP	back pressure
CCS	carbon capture and storage
CPA	cubic plus association
CT	computed tomography
CT_{dry}	CT number of dry core [HU]
CT_{exp}	CT number during experiment [HU]
CT_{wet}	CT number of fully wet core [HU]
D	Darcy
EoS	equation of state
f_{conv}	water conversion [%]
f_g	gas fractional flow [-]
f_w	water fractional flow [-]
MFC	mass flow controller
M_w	molecular weight [g/mol]
n_{H_2O}	total moles of water [mol]
P	pressure [MPa]
PT	pressure transducer
PV	pore volume
S_H	hydrate saturation [%]
S_w	water saturation [%]
S_{w+H}	water+hydrate saturation [%]
T	temperature [k]
TC	thermocouple
V_φ	volume of core porosity [mL]

■ GREEK CHARACTERS

φ	porosity
ρ	density of hydrate [g/mL]

■ SUBSCRIPTS AND SUPERSCRIPTS

exp	experimental
g	gas
H	hydrate
w	water

■ REFERENCES

(1) Gholami, R.; Raza, A.; Iglauer, S. Leakage risk assessment of a CO_2 storage site: A review. *Earth-Science Reviews* **2021**, *223*, No. 103849.

(2) Saravanan, A.; Senthil Kumar, P.; Vo, D.-V. N.; Jeevanantham, S.; Bhuvaneswari, V.; Anantha Narayanan, V.; Yaashikaa, P. R.; Swetha, S.; Reshma, B. A comprehensive review on different approaches for CO_2 utilization and conversion pathways. *Chem. Eng. Sci.* **2021**, *236*, No. 116515.

(3) Ahmad, S.; Li, Y.; Li, X.; Xia, W.; Chen, Z.; Ullah, N. Numerical analysis of CO_2 hydrate growth in a depleted natural gas hydrate formation with free water. *Greenhouse Gases: Science and Technology* **2019**, *9* (6), 1181−1201.

(4) Zhang, P.; Chen, X.; Zhang, L.; Li, S.; Chen, W.; Wu, Q.; Fan, S.; Bao, R.; Mu, C. Mobilization of water affecting formation and dissociation of hydrate in clay sediment. *Chemical Engineering Journal* **2023**, *455*, No. 140936.

(5) Fahed Qureshi, M.; Zheng, J.; Khandelwal, H.; Venkataraman, P.; Usadi, A.; Barckholtz, T. A.; Mhadeshwar, A. B.; Linga, P. Laboratory demonstration of the stability of CO_2 hydrates in deep-oceanic sediments. *Chemical Engineering Journal* **2022**, *432*, No. 134290.

(6) Schicks, J. M. Gas hydrates in nature and in the laboratory: necessary requirements for formation and properties of the resulting hydrate phase. *ChemTexts* **2022**, *8* (2), 13.

(7) Hosseini Zadeh, A.; Kim, I.; Kim, S. Characteristics of formation and dissociation of CO_2 hydrates at different CO_2-Water ratios in a bulk condition. *J. Pet. Sci. Eng.* **2021**, *196*, No. 108027.

(8) Kim, S.; Lee, K.; Lee, M.; Ahn, T. Data-Driven Three-Phase Saturation Identification from X-ray CT Images with Critical Gas Hydrate Saturation. *Energies* **2020**, *13* (21), 5844.

(9) Dong, H.; Sun, J.; Zhu, J.; Liu, L.; Lin, Z.; Golsanami, N.; Cui, L.; Yan, W. Developing a new hydrate saturation calculation model for hydrate-bearing sediments. *Fuel* **2019**, *248*, 27−37.

(10) Benmesbah, F. D.; Clain, P.; Fandino, O.; Osswald, V.; Fournaison, L.; Dicharry, C.; Ruffine, L.; Delahaye, A. Calorimetric study of carbon dioxide (CO_2) hydrate formation and dissociation processes in porous media. *Chem. Eng. Sci.* **2022**, *264*, No. 118108.

(11) Aghajanloo, M.; Yan, L.; Berg, S.; Voskov, D.; Farajzadeh, R. Impact of CO_2 Hydrates on Injectivity During CO_2 Storage in Depleted Gas Fields: A Literature Review. *Gas Sci. Eng.* **2024**, *123*, No. 205250.

(12) Song, Y.; Wang, S.; Yang, M.; Liu, W.; Zhao, J.; Wang, S. MRI measurements of CO_2−CH_4 hydrate formation and dissociation in porous media. *Fuel* **2015**, *140*, 126−135.

(13) Yang, M.; Song, Y.; Zhu, N.; Zhao, Y.; Liu, Y.; Jiang, L. Dynamic Measurements of CO_2 Flow in Water Saturated Porous Medium at Low Temperature Using MRI. *Energy Procedia* **2013**, *37*, 1267−1274.

(14) Lei, L.; Park, T.; Jarvis, K.; Pan, L.; Tepecik, I.; Zhao, Y.; Ge, Z.; Choi, J.-H.; Gai, X.; Galindo-Torres, S. A.; et al. Pore-scale observations of natural hydrate-bearing sediments via pressure core sub-coring and micro-CT scanning. *Sci. Rep.* **2022**, *12* (1), 3471.

(15) Aghajanloo, M.; Taghinejad Esfahani, S. M.; Voskov, D. V.; Farajzadeh, R. Influence of Water Saturation and Water Memory on CO_2 Hydrate Formation/Dissociation in Porous Media Under Flowing Condition. *Chem. Eng. J.* **2024**, *492*, No. 152455. Available at SSRN: https://ssrn.com/abstract=4739766

(16) Eftekhari, A. A.; Farajzadeh, R. Effect of Foam on Liquid Phase Mobility in Porous Media. *Sci. Rep.* **2017**, *7* (1), 43870.

(17) Holland, M.; Schultheiss, P. Comparison of methane mass balance and X-ray computed tomographic methods for calculation of gas hydrate content of pressure cores. *Marine and Petroleum Geology* **2014**, *58*, 168−177.

(18) Lu, Z.; Sultan, N. Empirical expressions for gas hydrate stability law, its volume fraction and mass-density at temperatures 273.15 to 290.15 K. *GEOCHEMICAL JOURNAL* **2008**, *42* (2), 163−175.

(19) Li, N.; Fan, Z.; Ma, H.; Jia, S.; Kan, J.; Sun, C.; Liu, S. Permeability of Hydrate-Bearing Sediment Formed from CO2-N2Mixture. *Journal of Marine Science and Engineering* **2023**, *11* (2), 376.

(20) Ferdows, M.; Ota, M. Density of CO_2 Hydrate by Monte Carlo Simulation. *Proceedings of the Institution of Mechanical Engineers, Part C: Journal of Mechanical Engineering Science* **2006**, *220* (5), 691−696.